Supporting Information

Insights into the Enhanced Cycling Stability of Cobalt-Free Single-Crystal Layered Oxide Cathodes at Elevated Voltage

Tiancheng Liu[a,c], Ke Fan[a,c], Changsheng Chen[a,c], Mingxia Dong[b], Yanping Zhu[a], Gao Chen[a], Jiangtong Li[a], Zezhou Lin[a], Liuqing Li[a], Ye Zhu[a], Huangxu Li[a] and Haitao Huang[a]*.

[a] Department of Applied Physics and Research Institute for Smart Energy, The Hong Kong Polytechnic University, Hong Kong SAR, China;

[b] BASF Shanshan Battery Materials Co., Ltd;

[c] These authors contributed equally.

Figure

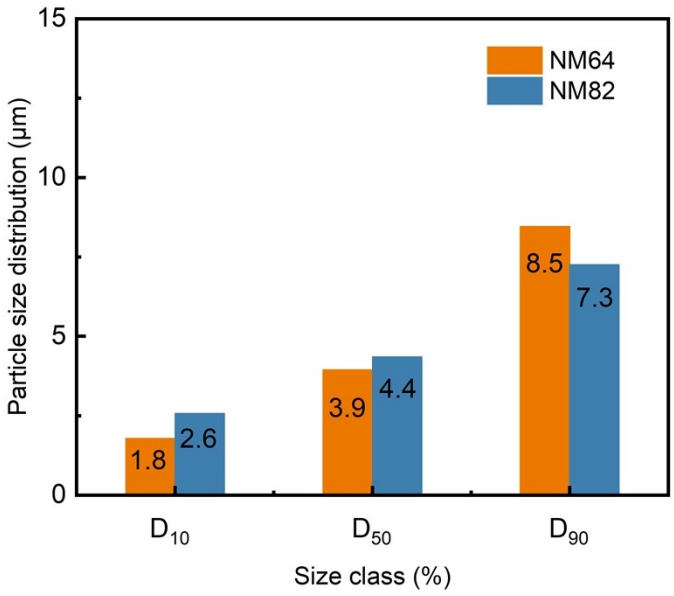

Figure S1. Particle size distribution of NM64 and NM82.

Compared to polycrystalline cathode, single-crystalline cathode exhibits relatively irregular morphology, leading to variations in cathode thickness in certain directions that may be smaller than the median diameter. Furthermore, the presence of particle

aggregates can lead to an overestimation of the measured particle size.

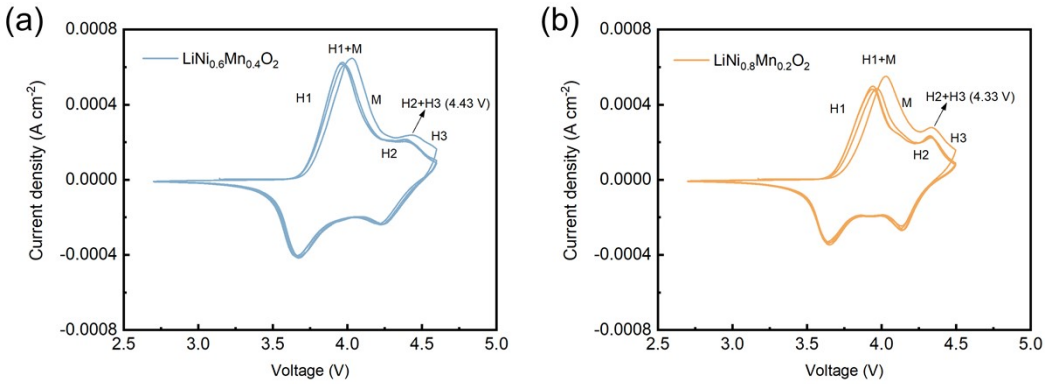

Figure S2. CV curves of (a) NM64 and (b) NM82 for the first four cycles.

Due to the more inactive Mn in NM64, the redox peaks shift to higher voltage in CV curves.

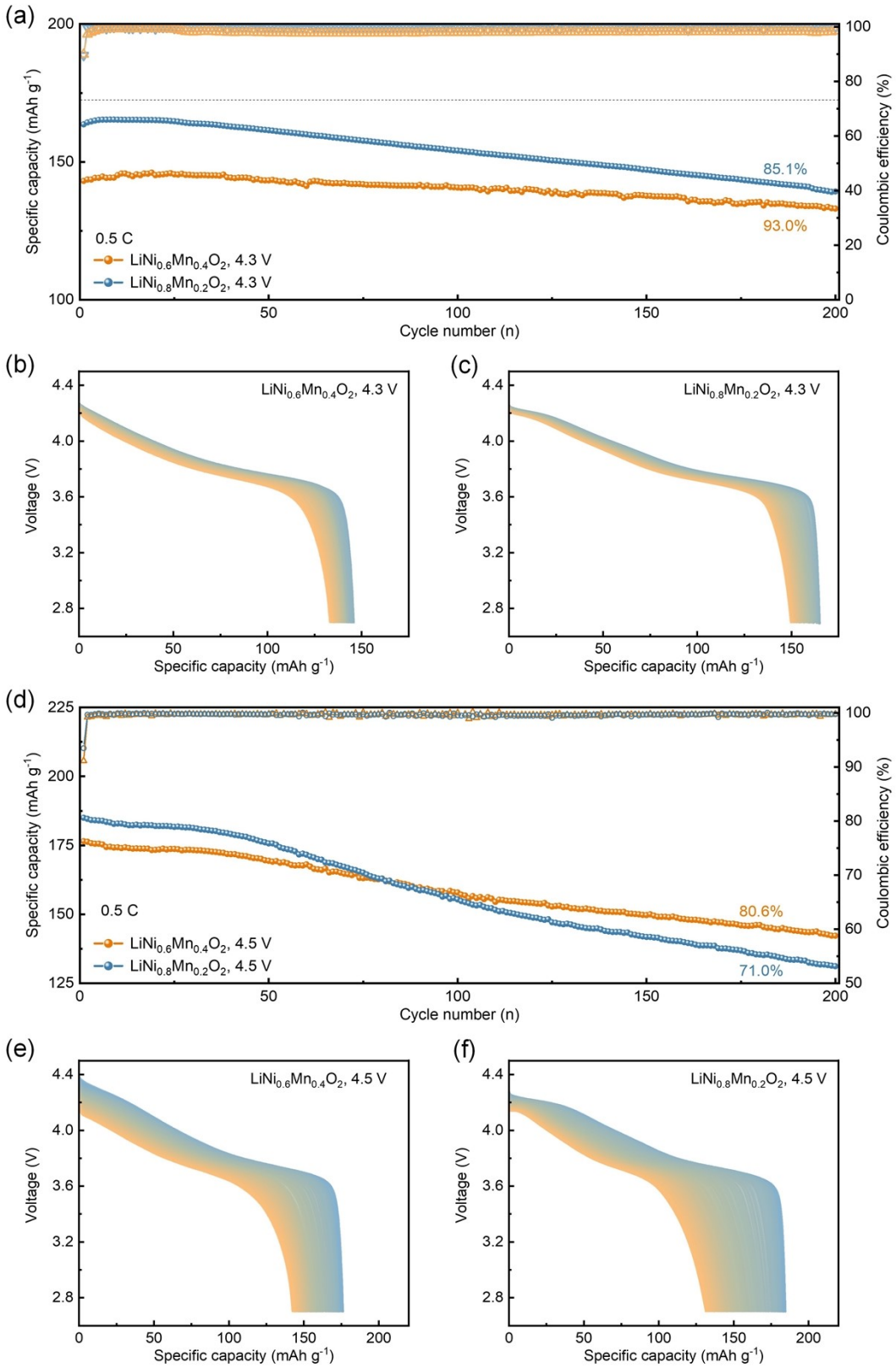

Figure S3. Electrochemical performance of NM64 and NM82 cathodes at 0.5 C. (a) Cycling performance of NM64 and NM82 in the voltage range of 2.7-4.3 V. Corresponding discharge profiles of (b) NM64 and (c) NM82. (d) Cycling

performance of NM64 and NM82 in the voltage range of 2.7-4.5 V. Corresponding discharge profiles of (e) NM64 and (f) NM82.

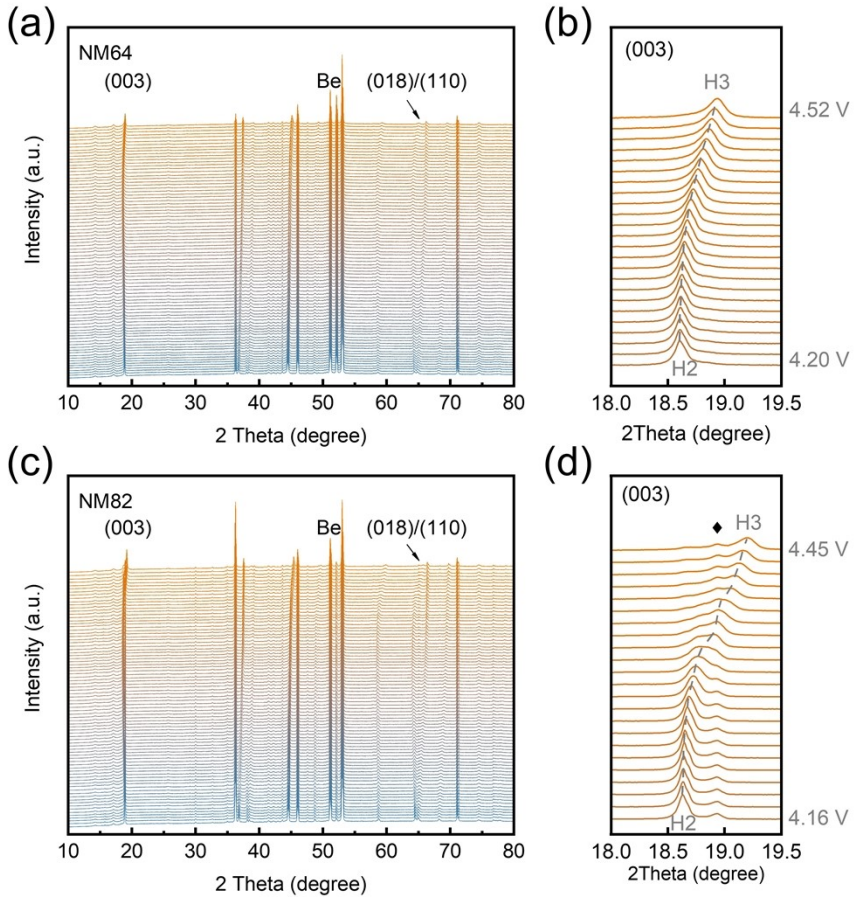

Figure S4. Full scale XRD patterns of (a) NM64 and (c) NM82 during charge process at 0.1 C rate. XRD patterns of (003) peak during H2-H3 phase transitions for (b) NM64 and (d) NM82 in the voltage range from 4.20 V to 4.52 V and from 4.16 V to 4.45 V, respectively.

In order to achieve an identical SOC of 220 mAh g^{-1}, The NM64 and NM82 were charged to 4.52 V and 4.45 V, respectively. "♦" can be identified to Fe_3O_4 from the stainless-steel cells.

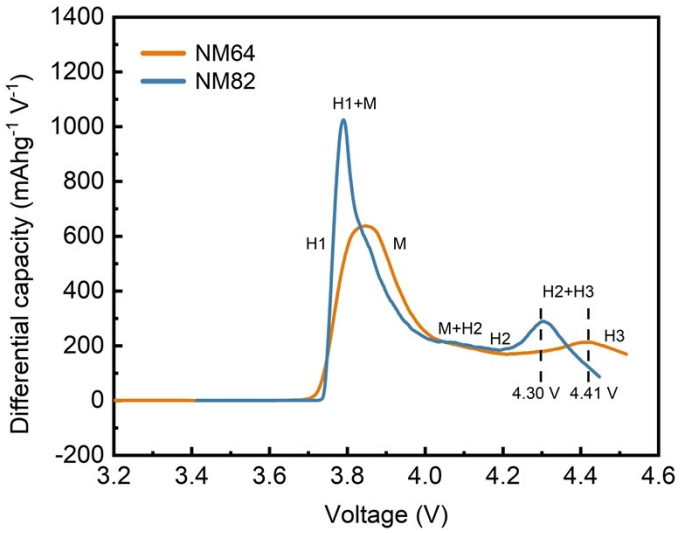

Figure S5. dQ dV^{-1} curves of NM64 and NM82 during the charge process to 220 mAh g^{-1} at 0.1 C for the in situ XRD tests. "H" refers to hexagonal phase and "M" refers to monoclinic phase. H2+H3 peak is located at 198.8 mAh g^{-1} (corresponding to 4.41 V) for NM64 while 191.8 mAh g^{-1} (corresponding to 4.30 V) for NM82.

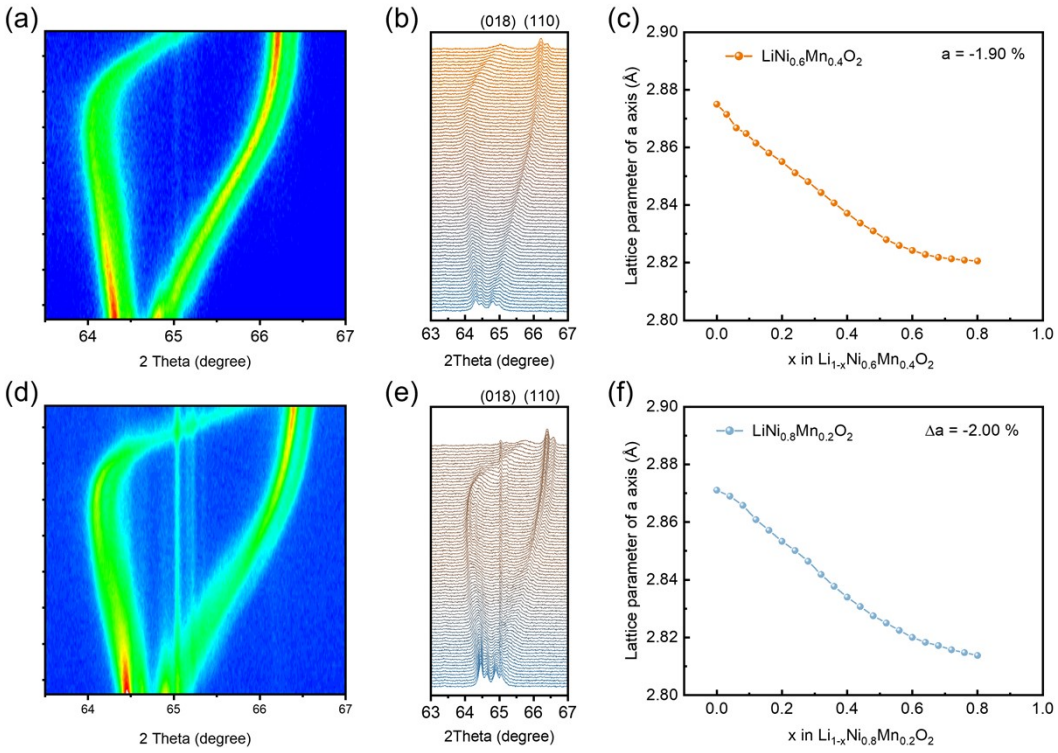

Figure S6. In situ XRD characterization during the first charge to 220 mAh g^{-1} at 0.1 C. Two-dimensional contour plots of (018)/(110) peaks for (a) NM64 and (d) NM82.

XRD patterns of (b) NM64 and (e) NM82. The corresponding lattice parameter of the *a*-axis of (c) NM64 and (f) NM82.

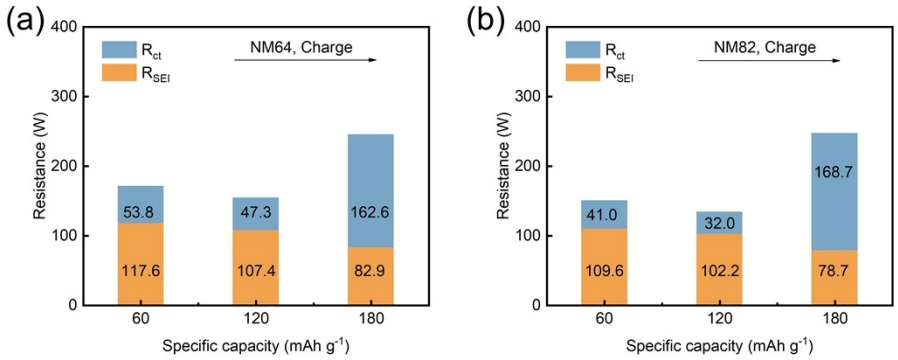

Figure S7. The fitting results of Nyquist Plot during various charge states of (a) NM64 and (b) NM82.

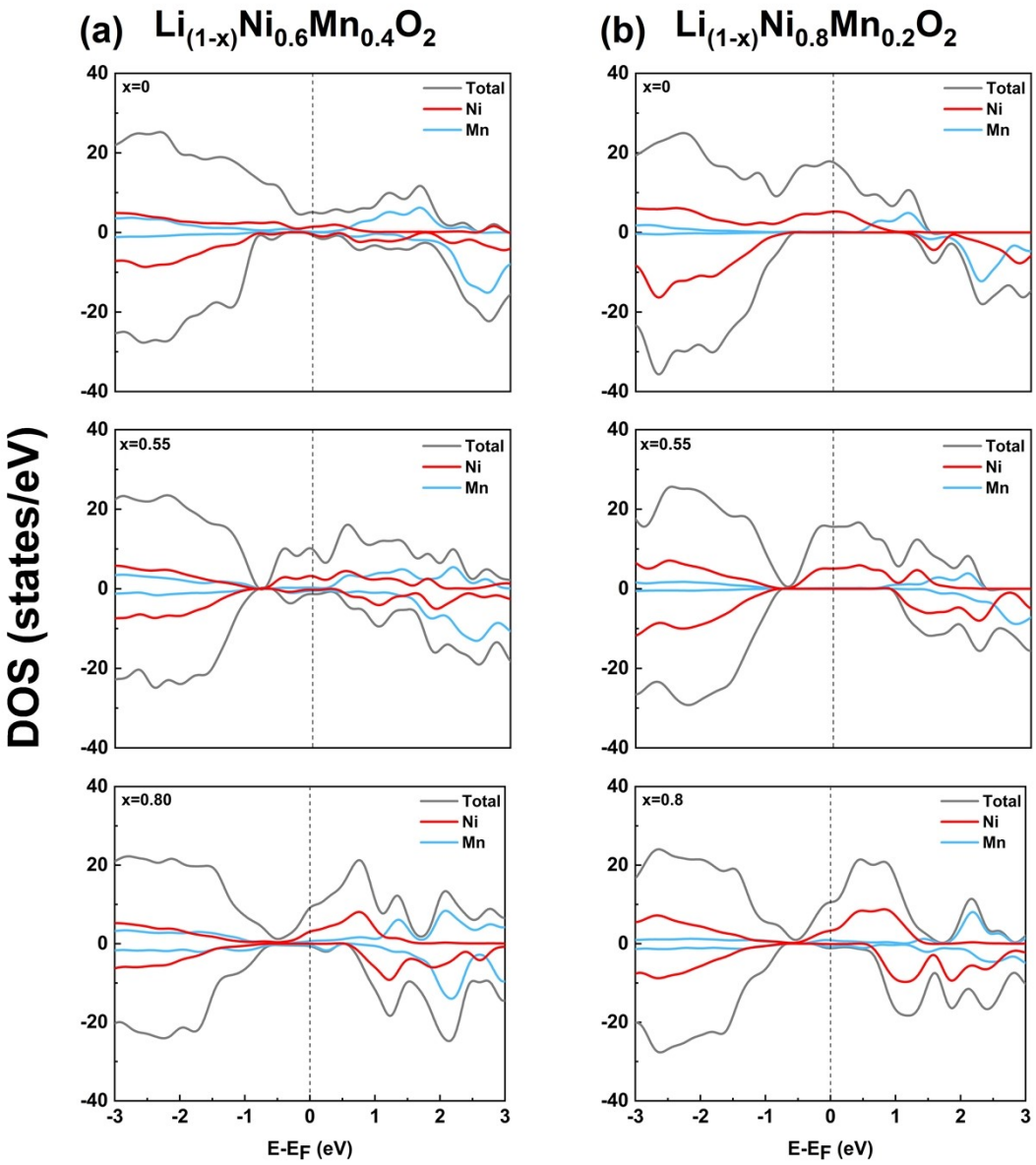

Figure S8. Density of states for (a) $Li_{(1-x)}Ni_{0.6}Mn_{0.4}O_2$ and (b) $Li_{(1-x)}Ni_{0.8}Mn_{0.2}O_2$. The Fermi level is set to zero and shown as the dashed line.

In order to obtain information about the changes of the valence states of Ni and Mn, the density of states (DOS) of Ni and Mn 3*d* orbitals in NM64 and NM82 (x = 0, 0.55, 0.80) are calculated. It's reported that the Ni is mainly responsible for the capacity contribution and Mn is inactive during charge and discharge process[1]. According to DOS results for pristine and delithiated states, Ni dominates the valance change during the whole process for both NM64 and NM82 cathodes, while the valance of Mn largely remains unchanged. Therefore, Ni is selected to carry out the XAFS tests.

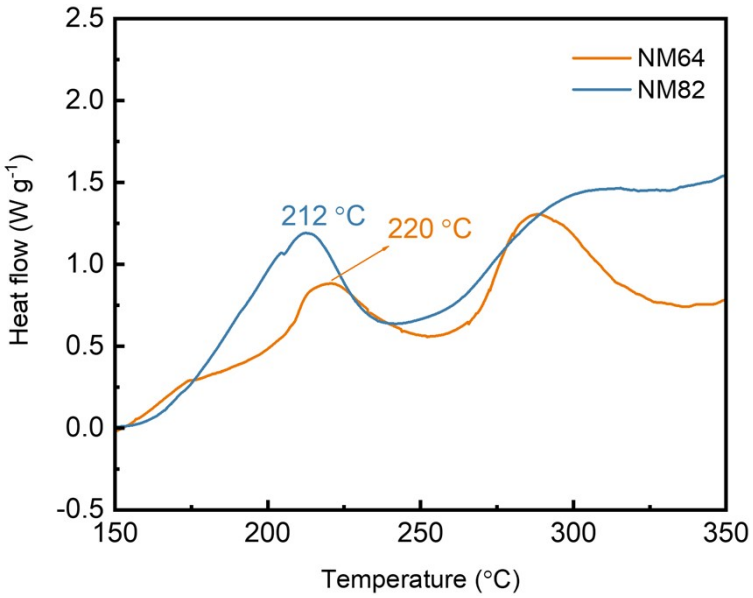

Figure S9. DSC curves of NM64 and NM82. The cathodes were charged to 220 mAh g^{-1}.

Table

Table S1. ICP-OES result of NM64 and NM82.

Element	Ni (mol %)	Mn (mol %)
NM64	60.9	39.1
NM82	80.9	19.1

Table S2. Cation occupancy and structural parameters based on XRD Rietveld refinement.

Sample	*a/b*-axis (Å)	*c*-axis (Å)	c/a	(003)/(104)	Li/Ni mixing
NM64	2.88179(4)	14.26582(4)	4.95032(7)	1.98	6.46%
NM82	2.87941(1)	14.23370(7)	4.94327(0)	1.73	3.82%

Reference

[1] T. C. Liu, L. Yu, J. J. Liu, J. Lu, X. X. Bi, A. Dai, M. Li, M. F. Li, Z. X. Hu, L. Ma, D. Luo, J. X. Zheng, T. P. Wu, Y. Ren, J. G. Wen, F. Pan, K. Amine, *Nature Energy* **2021**, 6, 277.